

Observation of femto-joule optical bistability involving Fano resonances in high- Q/V_m silicon photonic crystal nanocavities

Xiaodong Yang ^{a)}, Chad Husko, and Chee Wei Wong

Optical Nanostructures Laboratory, Columbia University, New York, NY 10027

Mingbin Yu, and Dim-Lee Kwong

The Institute of Microelectronics, 11 Science Park Road, Singapore Science Park II, Singapore, Singapore 117685

We observe experimentally optical bistability enhanced through Fano interferences in high- Q localized silicon photonic crystal resonances ($Q \sim 30,000$ and modal volume ~ 0.98 cubic wavelengths). This phenomenon is analyzed through nonlinear coupled-mode formalism, including the interplay of $\chi^{(3)}$ effects such as two-photon absorption and related free-carrier dynamics, and optical Kerr as well as thermal effects and linear losses. Our experimental and theoretical results demonstrate for the first time Fano-resonance based bistable states with switching thresholds of 185 μW and 4.5 fJ internally stored cavity energy (~ 540 fJ consumed energy) in silicon for scalable optical buffering and logic.

^{a)} Electronic mail: xy2103@columbia.edu

Two-dimensional photonic crystal (2D PhC) slabs confine light by Bragg reflection in-plane and total internal reflection in the third dimension. Introduction of point and line defects into 2D PhC slabs create localized resonant cavities and PhC waveguides respectively, with *ab initio* arbitrary dispersion control. Such defect cavities in high-index contrast materials possess strong confinement with subwavelength modal volumes (V_m) at $\sim (\lambda/n)^3$, corresponding to high field intensities per photon for increased nonlinear interaction. Moreover, cavities with remarkable high quality factors (Q) [1, 2] have been achieved recently, now permitting nanosecond photon lifetimes for enhanced light-matter interactions. The strong localization and long photon lifetimes in these high- Q/V_m photonic crystal nanocavities point to enhanced nonlinear optical physics, such as Lorentzian-cavity-based bistability [3-6] and Raman lasing [7, 8] in silicon photonics.

The interference of a discrete energy state with a continuum can give rise to sharp and asymmetric lineshapes, referred to Fano resonances [9, 10]. Compared to a Lorentzian resonance, these lineshapes arise from temporal pathways that involve direct and indirect (for example a resonance) transmission, with a reduced frequency shift required for nonlinear switching due to its sharper lineshape. If the indirect pathway can be further strongly localized (such as in a high- Q/V_m 3D cavity instead of a 1D Fabry-Perot cavity), the nonlinear characteristic switching thresholds can be further reduced. Optical bistability involving Fano resonances due to Kerr effect in photonic crystal cavities has been theoretically studied based on Green's function solution of Maxwell's equations [11]. Fano resonances have also been studied by transfer matrix technique [10, 12], and coupled-mode equations [13].

In this Letter, we present our measurements on Fano-based optical bistability as well as a temporal nonlinear coupled-mode framework for numerical analysis. Figure 1(a) shows a schematic of the theoretical model. A waveguide with two partially reflecting elements is side-coupled to a cavity. a is the amplitude of the cavity mode and s is the amplitude of the waveguide mode. With the coupled-mode formalism [14, 15], the dynamic equation for the amplitude $a(t)$ of the resonance mode is [13, 16]

$$\frac{da}{dt} = \left(-\frac{1}{2\tau_{total}} + i(\omega_0 + \Delta\omega - \omega_{wg}) \right) a + \kappa s_{a1+} + \kappa s_{a2+} \quad (1)$$

As shown in Figure 1(a), $s_{a1-} = \exp(-i\phi)s_{a2+} + \kappa a$ and $s_{a2-} = \exp(-i\phi)s_{a1+} + \kappa a$. $\phi = \omega_{\text{vg}} n_{\text{eff}} L / c$ is the phase shift. κ is the coupling coefficient between the waveguide mode $s(t)$ and $a(t)$, and $\kappa = i \exp(-i\phi/2) / \sqrt{2\tau_{\text{in}}}$ [16]. For a lossy partially reflecting element with the amplitude reflectivity r and transmissivity t , ($r^2 + t^2 \leq 1$) [14]

$$\begin{pmatrix} s_{aj+} \\ s_{aj-} \end{pmatrix} = \frac{1}{it} \begin{pmatrix} -(r^2 + t^2) & -r \\ r & 1 \end{pmatrix} \begin{pmatrix} s_{j+} \\ s_{j-} \end{pmatrix}, j = 1, 2 \quad (2)$$

In equation (1), the total loss rate for the resonance mode is $1/\tau_{\text{total}} = 1/\tau_{\text{in}} + 1/\tau_{\text{v}} + 1/\tau_{\text{lin}} + 1/\tau_{\text{TPA}} + 1/\tau_{\text{FCA}}$ [3,5,7]. The $\Delta\omega$ detuning of the cavity resonance from ω_0 is modeled due to the Kerr effect, free-carrier dispersion (FCD), and thermal dispersion effects under first-order perturbation. With the modeled carrier dynamics and thermal transients [7], the coupled nonlinear dynamical behavior of the Fano optical system is numerically integrated.

The optical system consisting of a photonic crystal waveguide side coupled to a high- Q/V_m nanocavity with five linearly aligned missing air holes ($L5$) in an air-bridge triangular lattice photonic crystal slab with thickness of $0.6a$ and the radius of air holes is $0.29a$, where the lattice period $a = 420$ nm, as shown in Figure 1(b). The shift S_l of two air-holes at cavity edge is $0.02a$ to tune the radiation mode pattern for increasing the Q factors. The waveguide-to-cavity separation is five layers of holes. The index contrast at the waveguide input and output facets act as partially reflecting elements with distance L of around 1.9 mm to form a Fabry-Perot resonator and perturb the phase of waveguide mode. Figure 1(c) shows the E_y field of the resonance mode mid-slab from 3D FDTD simulations.

The devices were fabricated with the standard integrated circuit techniques in a silicon-on-insulator substrate. A polarization controller and a lensed fiber are used to couple transverse-electric polarization light from tunable laser source into the waveguide. A second lensed fiber collects the transmission from the waveguide output that is sent to the photodetector and lock-in amplifier. The input power coupled to the waveguide is estimated from the transmitted power through the input lensed fiber, waveguide and the output lensed fiber [5]. The total transmission loss of the whole system is around 24.8 dB at wavelength of 1555 nm. At low input power of 20 μW , the measured resonant

wavelength λ_0 is 1556.805 nm. And the estimated Q , based on the full-width at half maximum (FWHM) $\Delta\lambda$ of 52 pm is around 30,000. From 3D FDTD method, the vertical Q factor Q_v is around 100,000 and the in-plane Q factor Q_{in} is around 45,000 so that the total Q factor $Q_{tot} = 1/(1/Q_v + 1/Q_{in}) = \sim 31,000$.

Figure 2(a) shows the measured transmission spectrum of the waveguide with different input powers. Each transmission shown is repeated over multiple scans. Sharp and asymmetric Fano lineshapes are observed. The spectral lineshapes depend on the position of cavity resonance in a Fabry-Perot background, highlighting Fano interference pathways. Here the spectra show ascending Fano resonances. The Fabry-Perot fringe spacing $d\lambda$ is around 230 pm, which corresponds to the distance between two waveguide facets $d = 1.902$ mm ($d = \lambda^2/(2*d\lambda*n_{eff})$ and effective index of 2.77 from FDTD simulations). As the input power increases, the Fano lineshapes were red-shifted due to two-photon-absorption induced thermo-optic nonlinearities in silicon [3-5]. Figure 2(b) shows the calculated transmission spectrum from nonlinear coupled-mode model with the input powers used in the experiment. All parameters used in calculation are from either reference papers or FDTD results [7]. When the input power is 1 μ W or less, the cavity response is in the linear regime. As the input power increases, the Fano lineshapes were red-shifted.

Figure 3(a) shows the observed hysteresis loop of Fano resonance at red detuning δ of 22 pm. The bistable loops of ascending Fano lineshapes are very distinct from Lorentzian lineshapes. Firstly, one suggestive indication is the asymmetry in the hysteresis loop, with sharp increase (gentle decrease) with increasing (decreasing) power for lower (upper) branch, resulting from the asymmetric Fano lineshape. Secondly, for ascending Fano resonances, an important indication is the upward slope (*increase* in transmission) for *increasing* input power for a side-coupled cavity. For a symmetric Lorentzian in a side-coupled drop cavity, a downward slope (or decrease in transmission) should be expected for increasing input power [17]. Thirdly, the dip in the transmission (as indicated by the dotted red circle in Figure 3(a)) is another signature of the Fano resonance. This feature is not observable with a symmetric Lorentzian and in fact is an aggregate result of the three self-consistent solutions of the nonlinear Fano system, such as predicted using Green's function method in Ref. 11. Our nonlinear coupled-mode theory framework

cannot trace out the individual solutions [11] but show the aggregate behavior, and is in remarkable agreement with our experimental measurements and the Green's function predictions.

The Fano bistable “off” power (p_{off}) is estimated at 147 μW and the “on” power (p_{on}) at 189 μW for a 22 pm detuning, as shown in Figure 3(a). These threshold powers are determined experimentally from half the total system transmission losses. From the 189 μW (147 μW) p_{on} (p_{off}) thresholds, this corresponds to an estimated internally stored cavity energy [3] of 4.5 fJ (1.5 fJ) based on a numerical estimate of waveguide-to-cavity coupling coefficient (κ^2) of 13.3 GHz. The consumed energy, in terms of definition used in Ref. 18, is ~ 540 fJ (60 fJ) based on the numerical estimated thermal relaxation time of 25 ns and 11.4 % (1.6 %) of input power absorbed by TPA process for “on” (“off”) state, although this could be much lower with minimum detuning to observe bistability. The femto-joule level switching in the stored cavity energy is due to the lowered threshold from the sharp Fano interference lineshape, the small mode volume and high- Q photonic crystal cavities. For the 22 pm detuning, the switching intensity contrast ratio is estimated at 3.5 dB (from the regions with sharp discrete bistable “jumps”) with a p_{on}/p_{off} ratio of 1.286. Figure 3(b) shows the calculated Fano bistable hysteresis at the detuning of 22 pm from nonlinear coupled-mode theory. The calculated p_{off} and p_{on} thresholds are 151 μW (with the stored cavity energy of 1.5 fJ) and 186 μW (4.5 fJ) respectively, in excellent agreement with the experimental results, with a switching contrast of 9.3 dB and p_{on}/p_{off} ratio of 1.232.

Now we examine parametrically the dependence of the Fano-type bistability against achievable device characteristics, with our developed nonlinear model. Figure 4 summarizes the extensive numerically-calculated effects of normalized-detuning ($\delta/\Delta\lambda$), mirror reflectivity r , cavity Q , and the position of cavity resonance on the characteristic threshold power p_{on} , and switching contrast. A baseline Q of 31,000, a r of 0.5 with 11% mirror loss, a λ_0 of 1556.805 nm, and a detuning of $\delta=\Delta\lambda$ is used. In Figure 4(a), the threshold power for the Fano bistability increases for increasing normalized detuning (further normalized shift of incident laser frequency from Fano resonance) due to the larger shift in resonance needed for bistable switching. The switching contrast *decreases* slightly with increasing detuning due to the reduced contrast in the transmission (see for

example Figure 2 on the slight reduction in “peaks” and “dips” contrast for increasing input power) at the higher input powers needed for the bistable operation. The red-filled symbols correspond to the current experimental parameters. This switching contrast can significantly increase when the mirror reflectivity r increases from 0.35 to 0.8 (at detuning of $\delta=\Delta\lambda$) at the expense of increasing p_{on} (Figure 4(b)). The increase in p_{on} is due to higher mirror reflectivity, resulting in lower power coupled into the Fano system. A limit of 0.35 is used because for smaller r , a combination of both Lorentzian and ascending Fano resonance starts to appear. For r greater than 0.8, the threshold power is high, approximately a few milli-watts.

Figure 4(c) plots the threshold power and the stored cavity energy with different cavity Q factors at detuning of $\delta=\Delta\lambda$ and $r=0.5$. Note that p_{on} shows a $(1/Q^{1.568})$ -dependence, while the stored cavity energy needed for bistable shows a $(1/Q^{0.674})$ -dependence, highlighting the difference with a Lorentzian-type bistability where a $1/Q^{1.615}$ and $1/Q^{0.678}$ -dependence is found respectively by setting $r=0$ in the numerical simulations. The smaller exponential in the Fano system depicts a smaller improvement in threshold and cavity energy with increasing Q , or a less stringent requirement for higher cavity Q in Fano-type systems in contrast to Lorentzian-type systems. We also note that direct comparisons between an ascending Fano-type bistability and a Lorentzian-type bistability are difficult because the Fano system depends on multiple parameters; at specific parameters, it performs better (such as with p_{on} or switching contrast as possible parameters) and at other parameters, vice versa. For cavity Q factor of 1 million, the Fano threshold power is estimated at 2 μW , which corresponds to the stored cavity energy of 0.53 fJ. This stored cavity energy is much lower than a Fano resonance with cavity Q of 31,000 (4.5 fJ).

Figure 4(d) illustrates the influence of different position of cavity resonance λ relative to experimental λ_0 within the half period of Fabry-Perot background $d\lambda/2$ with $Q=31,000$, $r=0.5$, and $\delta=\Delta\lambda$, where the limits of $(\lambda-\lambda_0)/(d\lambda/2)$ are from -0.9 to 0.1 for ascending Fano resonances. These limits are chosen because they cover the region where the ascending Fano resonances are dominant over the Lorentzian or the descending Fano resonances. For ascending Fano resonances, p_{on} decreases as the cavity resonance λ shifts from the Fabry-Perot background maximum to its minimum. However, the switching contrast has

a maximum at a region between the maximum and minimum Fabry-Perot background, illustrating an interesting trade-off when selecting an optimum set of Fano-type bistable operating parameters.

In this work we demonstrate experimentally for the first time all-optical bistability arising from sharp Fano resonances in high- Q/V_m silicon photonic crystal nanocavities. Using the two-photon-absorption induced thermo-optic nonlinearity, an “on”-state threshold of 189 μW and stored cavity energy of 4.5 fJ is observed, and in good agreement with the nonlinear coupled-mode formalism. Although the thermo-optic is slow (on order of μs), other nonlinear mechanisms such as two-photon-absorption induced free-carrier dispersion [3,4,6] can remarkably achieve ~ 50 ps switching in silicon. The threshold power can be further reduced to the μW level (or sub-fJ of stored cavity energy) with higher- Q/V_m nanocavities or further optimization of the detuning for reduced threshold and large contrast ratio. Our first observations of Fano-type bistability highlight the feasibility of an ultra-low energy switching mechanism in monolithic silicon benefiting from the sharp Fano lineshapes, for scalable functionalities such as all-optical switching, memory, and logic for information processing.

This work was partially supported by the National Science Foundation (awards ECS-0622069 and ECS-0508343) and Columbia University Initiatives in Science and Engineering for Nanophotonics. X. Yang acknowledges the support of an Intel Fellowship.

References

1. B. S. Song, S. Noda, T. Asano, and Y. Akahane, *Nat. Mater.* **4**, 207 (2005).
2. E. Kuramochi, M. Notomi, S. Mitsugi, A. Shinya, T. Tanabe, and T. Watanabe, *Appl. Phys. Lett.* **88**, 041112 (2006).
3. P. E. Barclay, K. Srinivasan, and O. Painter, *Opt. Express* **13**, 801 (2005).
4. T. Tanabe, M. Notomi, S. Mitsugi, A. Shinya, E. Kuramochi, *Appl. Phys. Lett.* **87**, 151112 (2005).
5. T. Uesugi, B. Song, T. Asano, and S. Noda, *Opt. Express* **14**, 377 (2006).
6. V. R. Almeida, C. A. Barrios, R. R. Panepucci and M. Lipson, *Nature* **431**, 1081 (2004).
7. X. Yang and C. W. Wong, to be published in *Opt. Express*, (2007).
8. H. Rong, R. Jones, A. Liu, O. Cohen, D. Hak, A. Fang and M. Paniccia, *Nature* **433**, 725 (2005).
9. U. Fano, *Phys. Rev.* **124**, 1866 (1961).
10. S. Fan, *Appl. Phys. Lett.* **80**, 908 (2002).
11. A. R. Cowan and J. F. Young, *Phy. Rev. E* **68**, 046606 (2003).
12. V. Lousse and J. P. Vigneron, *Phy. Rev. B* **69**, 155106 (2004).
13. S. Fan, W. Suh and J. D. Joannopoulos, *J. Opt. Soc. Am. A* **20**, 569 (2003).
14. H. A. Haus, *Waves and Fields in Optoelectronics*. (Prentice-Hall, Englewood Cliffs, N.J., 1984).
15. A. Yariv, *Optical Electronics*. (Sanders College Publishing, Philadelphia, PA., 1991).
16. B. Maes, P. Bienstman and R. Baets, *J. Opt. Soc. Am. B* **22**, 1778 (2005).
17. M. F. Yanik, S. Fan, and M. Soljačić, *Appl. Phys. Lett.* **83**, 2739 (2003).
18. M. Notomi, A. Shinya, S. Mitsugi, G. Kira, E. Kuramochi, and T. Tanabe, *Opt. Express* **13**, 2678 (2005).

Figure captions

Fig. 1. (a) Schematic of optical system including a waveguide side-coupled to a cavity. Two partially reflecting elements are placed in the waveguide. (b) SEM of photonic crystal $L5$ point-defect cavity side-coupled to line-defect waveguide. The input and output facets of the high-index-contrast waveguide form the partially reflecting elements. (c) E_y -field of the resonance mode mid-slab from 3D FDTD simulations.

Fig. 2. Measured (a) and CMT-calculated (b) transmission spectrum at different input powers, illustrating the asymmetric lineshapes. The side-coupled $L5$ cavity has a total Q of $\sim 30,000$.

Fig. 3. (a) Measured and (b) CMT-calculated asymmetric hysteresis loops for Fano resonance at a detuning of 22 pm. The red-circled region in panel (a) highlights a dip in transmission with increasing input power, a signature not present in Lorentzian-type resonances, and indicative of nonlinear Fano-type solutions. The arrows depict ascending and descending input powers to the Fano system.

Fig. 4. CMT calculated effects of (a) the wavelength detuning δ , (b) mirror reflectivity r , (c) cavity Q factor, and (d) the position of cavity resonance on the switching threshold power p_{on} and switching contrast. (The red-filled symbols correspond to the experimental parameters.)

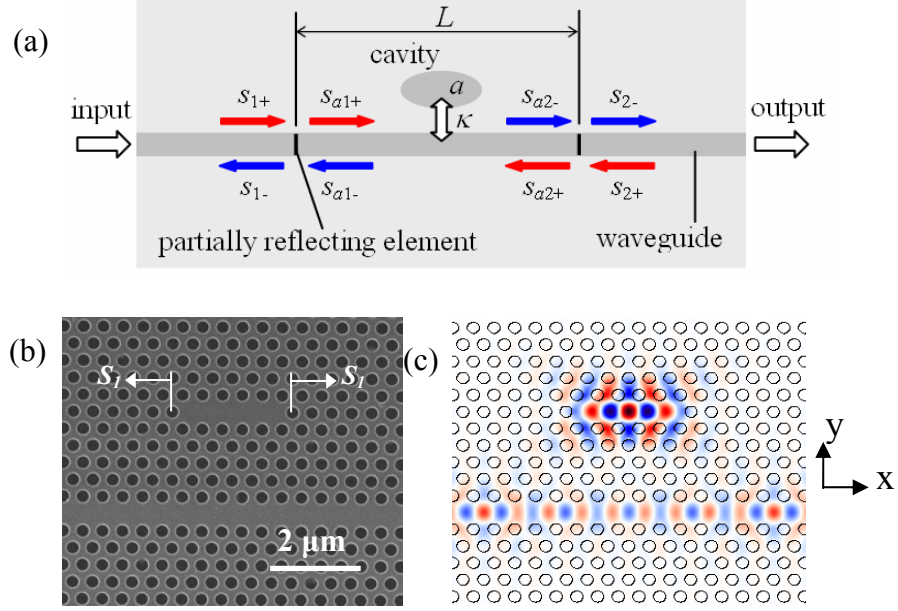


Fig. 1. (a) Schematic of optical system including a waveguide side-coupled to a cavity. Two partially reflecting elements are placed in the waveguide. (b) SEM of photonic crystal $L5$ point-defect cavity side-coupled to line-defect waveguide. The input and output facets of the high-index-contrast waveguide form the partially reflecting elements. (c) E_y -field of the resonance mode mid-slab from 3D FDTD simulations.

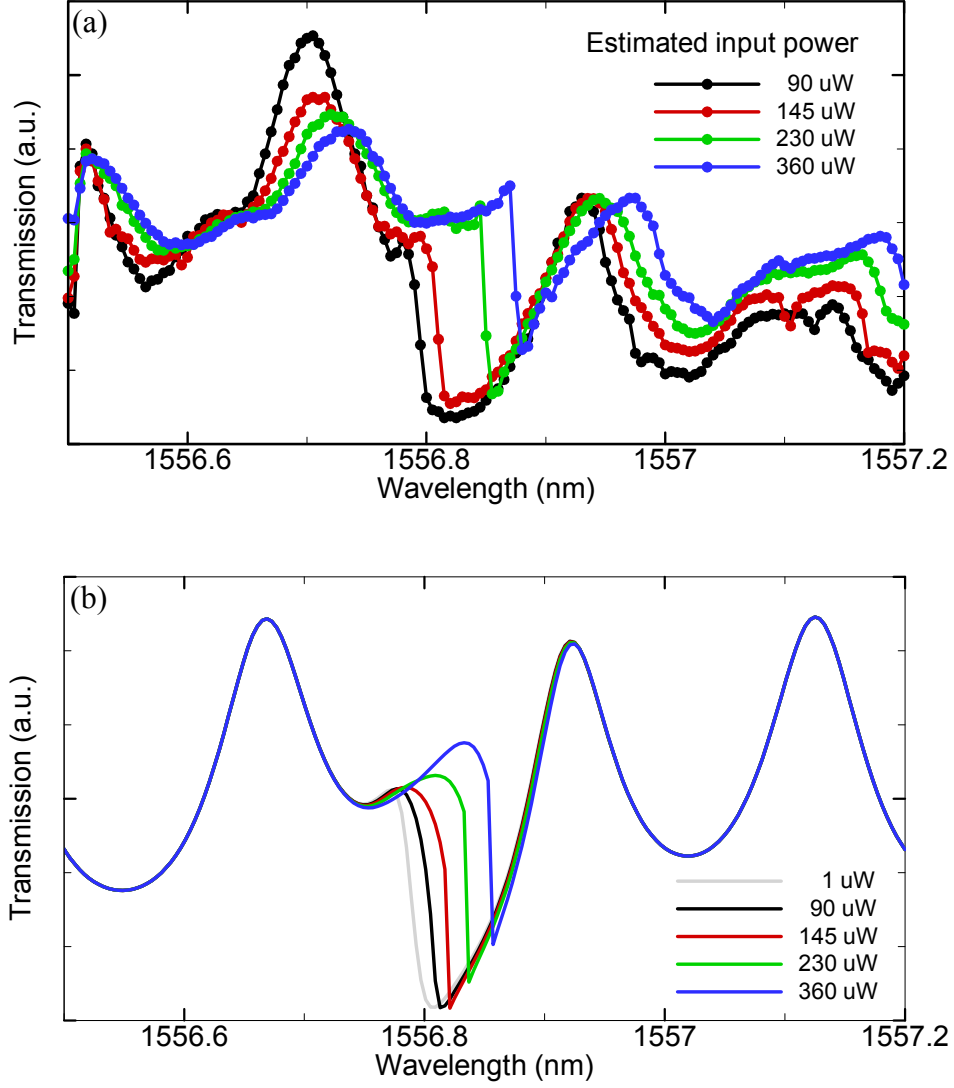


Fig. 2. Measured (a) and CMT-calculated (b) transmission spectrum at different input powers, illustrating the asymmetric lineshapes. The side-coupled $L5$ cavity has a total Q of $\sim 30,000$.

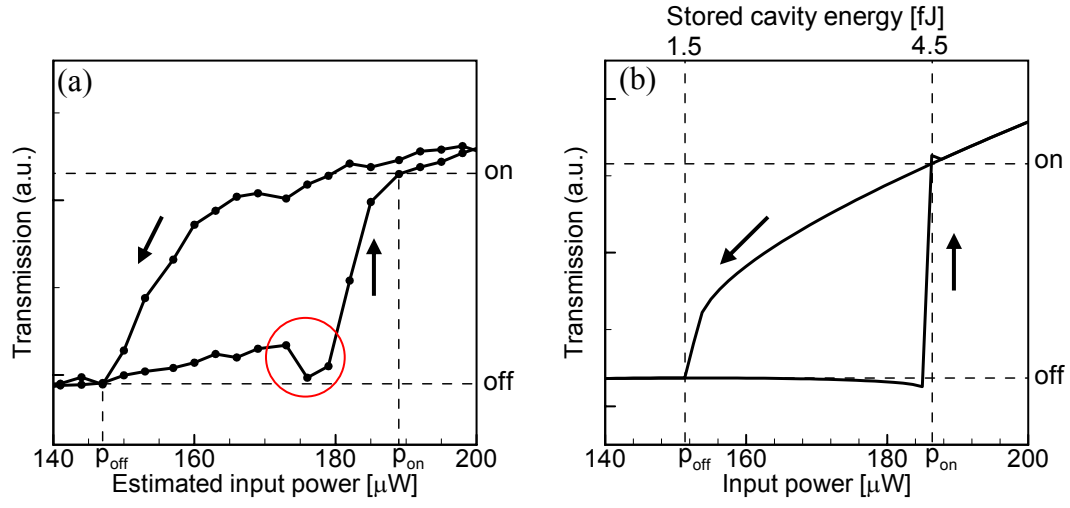


Fig. 3. (a) Measured and (b) CMT-calculated asymmetric hysteresis loops for Fano resonance at a detuning of 22 pm. The red-circled region in panel (a) highlights a dip in transmission with increasing input power, a signature not present in Lorentzian-type resonances, and indicative of nonlinear Fano-type solutions. The arrows depict ascending and descending input powers to the Fano system.

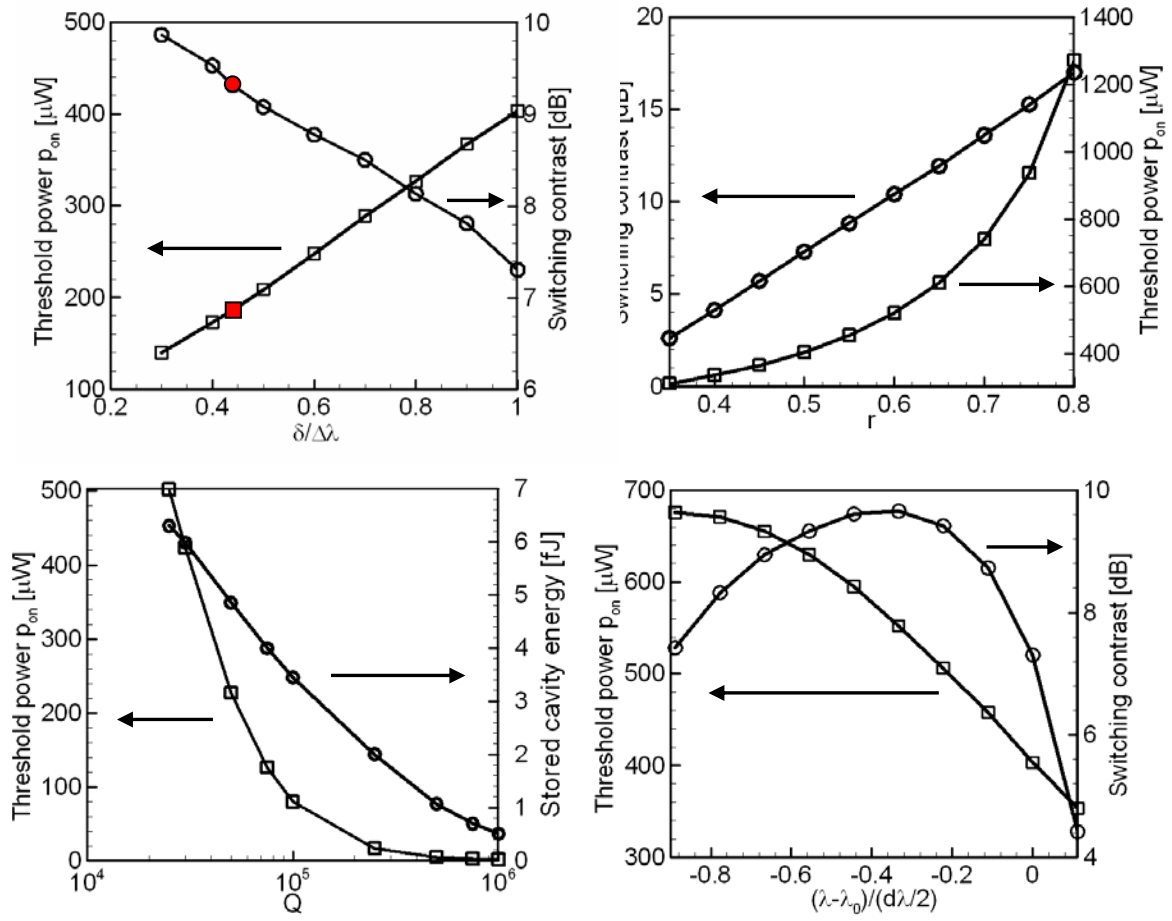


Fig. 4. CMT calculated effects of (a) the wavelength detuning δ , (b) mirror reflectivity r , (c) cavity Q factor, and (d) the position of cavity resonance on the switching threshold power p_{on} and switching contrast. (The red-filled symbols correspond to the experimental parameters.)